Growth and characterisation of titanium sulfide nanostructures by surface-assisted vapour transport methods; from trisulfide ribbons to disulfide nanosheets.

S. J. Denholme,[a,b] P. Dobson,[b] J. M. R. Weaver,[b] I. MacLaren[c] and D. H. Gregory[a]*

a WestCHEM, School of Chemistry, University of Glasgow, Glasgow, G12 8QQ
b School of Engineering, University of Glasgow, Glasgow, G12 8QQ
c School of Physics & Astronomy, University of Glasgow, Glasgow, G12 8QQ
E-mail: salden@chem.gla.ac.uk, p.dobson@elec.gla.ac.uk, j.weaver@elec.gla.ac.uk, ian.maclaren@glasgow.ac.uk, Duncan.Gregory@glasgow.ac.uk

Abstract: Surface Assisted Chemical Vapour Transport (SACVT) methods have been employed to grow nanostructures of titanium disulfide (TiS_2) and titanium trisulfide (TiS_3). SACVT reactions occur bewteen titanium and sulfur powders to form TiS_x species transported in the vapour phase to grow nanometric flower-like structures on titanium-coated silica substrates. The evolution of structure and composition has been followed by powder X-ray diffraction, electron microscopy and Raman spectroscopy. At 1:2 Ti:S ratios, the size and shape of the hexagonal 1T-TiS_2 titanium disulfide structures formed can be varied from flower-like growths with "petals" formed from nanosheets 10 nm thick to platelets microns across. Increasing the proportions of sulfur (Ti:S 1:4) enables TiS_3 flower-like structures composed of radiating nanoribbons to grow at elevated temperatures without decomposition to TiS_2. TEM/SAED suggests that individual trisulfide ribbons grow along the [010] direction. Magnetic properties of the disulfide nanomaterials have been determined using SQUID magnetometry and Raman spectra for disulfides suggest that their crystal and electronic structures may be more complex than expected for bulk, stoichiometric, CdI_2-structured TiS_2.

Keywords: Titanium, sulfur, synthesis, growth, vapour transport, electron microscopy , structure, Raman spectroscopy, magnetism

Reference for publisher use only

Biographical notes:

Saleem J. Denholme obtained an honours degree in Chemistry in 2007 at the University of Glasgow where he is currently studying for a PhD under the supervision of Prof. Duncan H Gregory. His research interests focus on the synthesis, properties and applications of many transition metal-chalcogenide systems.
Phillip Dobson obtained his BSc (1997) and PhD (2001) in Chemistry at Warwick University before moving to Glasgow to work on bespoke AFM probes. Since this time he has expanded his research to include aspects of nanofabrication, micro-mechanics and

nanomaterials. In 2005 he gained a Research Councils UK (RCUK) Research Fellowship in the Faculty of Engineering, University of Glasgow with his research focusing on microthermal devices and carbon nanotube growth. He is currently researching a variety of areas including AFM, micro-mechanics, nano-material composites and novel nano-metrology systems.

John M. R. Weaver has been active in the area of nano scale measurement since 1988 when he developed the scanning tunnelling thermocouple and potentiometric AFM. He leads an effort in the development of generalised nanocharacterisation systems based on the electron-beam lithographic functionalisation of AFM probes, including systems for extremely accurate thermal measurement. He is also actively involved in the development of lithographic methods for the production of nanostructures at the 1nm scale. He led the construction of the James Watt Nanofabrication Centre, a 750m^2 facility for the fabrication of complex nanosystems, which opened in 2006.

Ian MacLaren graduated from the University of Birmingham with a PhD in Metallurgy and Materials in 1995. His work since then has concentrated upon the application of transmission electron microscopy for the characterisation of inorganic materials and he is currently lecturer in Solid State Physics in the School of Physics and Astronomy.

Duncan H. Gregory studied at the University of Southampton completing his PhD in solid state chemistry in 1993 under Prof. Mark Weller. He was an EPSRC Advanced Fellow, Lecturer and Reader in Materials Chemistry at the University of Nottingham until 2006. He then took up the WestCHEM Chair in Inorganic Materials at the University of Glasgow and is currently Head of Inorganic Chemistry in the School of Chemistry. His research interests centre on non-oxides and nanomaterials with potential applications in areas including sustainable energy and electronics.

1 Introduction

The layered CdI_2-type structure and redox chemistry of titanium disulfide (1T-TiS_2) have collectively encouraged its study as a host for intercalation over many years [1-8]. These possibilities have promoted a thorough investigation of intercalation-driven properties, which have been extended into the nano-regime. TiS_2 nanotubes have been investigated for both their hydrogen storage and lithium intercalation capabilities, for example [9, 10]. By contrast, the chemistry and physical properties of titanium trisulfide, TiS_3, are relatively unexplored since earlier work investigating crystal and electronic structure [11,12]. TiS_3 is reported as forming the monoclinic $ZrSe_3$ structure containing infinite chains of distorted trigonal Ti-S prisms aligned parallel to the monoclinic *b* axis and is semiconducting with a band gap of 0.9 eV. More recent work has demonstrated that it is possible to grow nanobelts of TiS_3 which demonstrate both high tensile strength and field emission properties [13, 14].

Growth studies rely on the development of methods to produce nanostructured titanium sulfides controllably and reproducibly. For example, previously TiS_2 nanomaterials have been produced by precursor reduction-sulfurisation reactions such as in the preparation of TiS_2 nanotubes with inner diameters of 10 nm and lengths of up to 5 μm by the reaction of a $TiCl_4$ precursor with H_2S and H_2 gas [15]. There are only a small number of instances however where chemical vapour deposition (CVD) techniques have been adopted to synthesise nano-TiS_2 successfully, but those that exist have produced

some startlingly unusual results in which nanoscale component (primary) structures build up complex secondary structures; two examples being dendritic crystals and flower like structures [16,17]. (In fact, very similar flower-like structures have also recently been achieved by wet-chemical synthesis [18]). These dendrites and flowers both originate from stoichiometric quantities of the powdered elements. The arrays of nanoflowers additionally then require a titanium foil substrate to enable growth. Investigations have identified optimum temperatures and reaction times to achieve the best results for consistent morphology, crystallinity and purity of the phase. In fact, a growth substrate was also used very effectively in an earlier study, which generated whiskers of TiS_2 by utilising an Ni-coated Si wafer [19]. In this case, the substrate was placed between separate elemental sulfur and titanium sources and the synthesis was conducted under a stream of Argon. The nickel at the surface of the wafer is reported to function as a catalyst in a vapour-liquid-solid (VLS) mechanism leading to the growth of stoichiometric TiS_2 whiskers with diameters ranging from 100 -200 nm.

Growth of nanostructured TiS_3 has been thus far confined to chemical vapour transport (CVT) routes [13,14] exploiting the ability of TiS_3 to grow on Ti foil surfaces in much the same way as, for example, TaS_2 will grow on a tantalum metal surface [20]. Both reports yield arrays of bundled nanobelts of TiS_3 and, in fact, thin films of TiS_3 were reported to form under low temperature conditions *via* MOCVD with a $TiCl_4$ precursor a decade earlier, although the microstructure of the trisulfide products was not investigated in detail [21].

It is a focus of our research to design and adapt CVT and CVD methods with the intent of exerting a greater control over their outcome [20,22]. Metal surfaces can be employed very successfully as a growth medium in Surface Assisted Chemical Vapour Transport (SACVT) reactions but SACVT methods are not uniformly appropriate across all metal-chalcogenide systems and one has to recognise the limitations imposed by the high melting points of many transition metals and their compounds. This has led us in previous work to develop physical vapour transport (PVT) methods in which the chalcogen is utilised in the vapour phase to grow nanostructures on a suitable metal substrate [23]. The rationale is thus that the chalcogen vapour can participate in reactions *via* vapour-solid or vapour-liquid-solid mechanisms at the metal surface. In principle, in this way one could design and template the nanomaterials by patterning the metal substrate with high precision.

Here we describe surface assisted PVT (SAPVT) and SACVT experiments in which Ti films on SiO_2 wafer substrates are reacted with either S or Ti-S vapour to produce various Ti-S compositions and morphologies, principally as a function of temperature. The techniques permit control of phase, crystal structure and morphology and it is possible to follow the growth of Ti-S nanostructures from clusters of ribbons of TiS_3 to nanoflowers of TiS_2 composed of nanosheet “petals” of the order of 10 nm in thickness.

2. Experimental

3.1 Fabrication of metal films

High purity titanium films were produced by evaporation techniques. Nanometric layers of metal were deposited on to a silica support using a Plassys MEB 400S electron beam evaporator under a chamber pressure of 1×10^{-7} mbar. Under these conditions, in these experiments we were able to deposit titanium as 50 nm films with a high degree of precision. Film metathickness was determined during deposition *via* an in-chamber quartz crystal sensor.

3.2 Synthesis of Ti-S nanostructures

Titanium sulfide nanomaterials were synthesised by the reaction of the SiO_2-supported Ti thin films with chalcogen or Ti-S vapour in sealed silica reaction tubes designed in-house for vapour transport chemistry (Fig. 1) [20]. Weighed amounts of sulfur (Fisher, 99.99%) and titanium (Koch-Light Laboratories, 99.95%) powders were placed in one end of a 12 mm diameter silica reaction tube prior to the introduction of the central constriction. The Ti coated substrate, of known film thickness (50 nm) and substrate area ($2cm^2$), was then placed in the opposite end of the silica tube before the ampoule was sealed under vacuum to a pressure of 3 mbar (using a two-stage Edwards rotary pump equipped with Pirani gauge).

Figure 1 Experimental set up for vapour transport reactions; the Ti-coated silica substrate and reactant powders are located in the opposite ends of an evacuated, constricted silica ampoule.

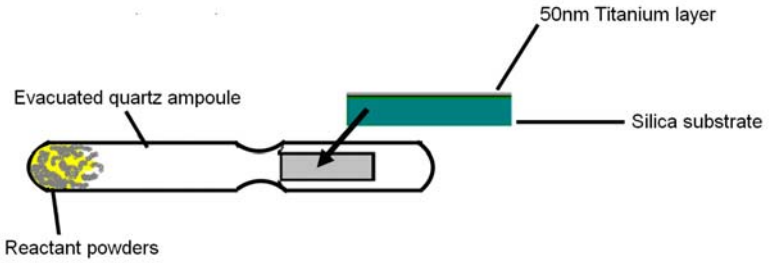

Reaction ampoules were heated in a box furnace to a set reaction temperature for varying amounts of time. The temperature was increased at 200 ºC h^{-1} for each heating step. Once reactions were complete, samples were left to cool in the furnace overnight. Samples were prepared under the conditions specified in Table 1.

Table 1 Ti-S sample synthesis conditions

Sample No.	Reactant powders; mass / g	Ti film thickness / nm	Reaction T / ºC	Reaction time/hrs	Rate of cooling / ºC h^{-1}
1	S; 0.01	50	650	60	50
2	S; 0.01	50	650	60	50
3	Ti,S; 0.014,0.02	50	650	60	50
4	Ti,S; 0.014,0.02	50	300	24	Air Quenched
5	Ti,S; 0.014,0.02	50	400	24	Air Quenched
6	Ti,S; 0.014,0.02	50	500	24	Air Quenched
7	Ti,S; 0.014,0.02	50	600	24	Air Quenched
8	Ti,S; 0.014,0.02	50	700	24	Air Quenched
9	Ti,S; 0.014,0.04	50	500	24	Air Quenched

3.3 Characterisation

Products (**1** - **9**) were retained on the substrate for analysis unless otherwise noted. Powder X-ray diffraction (PXD) analysis was performed using a PANalytical X'pert PRO MPD powder diffractometer in flat plate geometry. Samples were loaded onto a flat glass disk and secured using double-sided tape. Diffraction data were typically collected for 5 ° ≤ 2θ ≤ 85 ° with a 0.017 ° step size with scan times of from 1 - 12 h with a sample stage rotation of 15 RPM. Small sample volumes required that PXD analysis allowed for the high intensity reflections from the underlying silica substrate. Alternative methods of loading samples were attempted to try and reduce or remove substrate effects but best results were obtained from the method described above and characterisation of unique sample reflections was possible via this method. Diffraction data were compared to patterns in the ICDD (JCPDS) powder diffraction file (PDF) using the PANalytical High Score Plus software package. Additional data for (**1** - **9**) as appropriate were collected overnight (15 h; 5 ° ≤ 2θ ≤ 85 ° with a step size of 0.017 °) for indexing using the DICVOL software package [24] and least squares cell parameter refinement.

Scanning electron microscopy (SEM) was performed using two instruments; a Philips XL30 ESEM and a Hitachi S4700 cold field emission gun SEM. Typically, samples were loaded onto aluminium stubs using adhesive carbon tabs and run in high vacuum mode with an applied accelerating voltage of 15 kV and a working distance of 12.5 mm for imaging and 20 kV and a working distance of 10 mm for energy dispersive X-ray analysis, (EDX). EDX analysis was performed within the Philips instrument using an Oxford instruments 7200 EDX spectrometer in order to determine elemental compositions (which can be obtained with accuracy for elements of atomic number from carbon upwards). Transmission electron microscopy was performed using a FEI Tecnai T20 (FEI, Eindhoven, Netherlands) operated at 200 kV acceleration voltage using a LaB6 filament with images recorded using a Megaview III CCD camera (Olympus SIS GmbH, Garching, Germany). Conventional bright field and dark field diffraction contrast imaging was used in combination with selected area diffraction to characterize the nanostructure and relate this to the crystallography of the materials. Samples for SEM of sufficient thickness were prepared by depositing powder on to a carbon tab. Samples for

TEM were prepared by sonicating the powders in ethanol and then pipetting drops of the suspension onto holey carbon film Cu grids.

Raman spectra were collected at room temperature using a Horiba LabRAM HR confocal microscope system with a 532 nm green laser. A hole aperture of 50 um, 600 gr/mm grating and a Synapse CCD detector were used.

Magnetic measurements were performed using a Quantum Design MPMS 5T SQUID magnetometer. Samples were loaded into degassed gelatine capsules. Field cooled (FC) and zero field cooled (ZFC) measurements were performed with an applied field of 100 Oe between 2 - 300 K. All magnetic data were corrected for the gelatine capsules and for core diamagnetism.

Results and Discussion

Our work follows from our earlier investigation into the nickel-sulfur system, where a set of suitable SAPVT reaction conditions were established to produce an array of highly symmetrical, isotropic structures of nickel disulfide (NiS_2) [23]. It was shown that a stark variation in structure occurred in a temperature range of 450 – 550 °C, culminating in the formation of individual nickel disulfide nanocubes at 650 °C. Following this precedent, our initial synthetic experiments employed analogous conditions in a preliminary SAPVT study of the titanium-sulfur system.

Trial reactions (**1–2**) showed that the outcome was difficult to control. Under these conditions there were indications that reaction was far from complete and sections of the surface was free of products (Fig 2). EDX of sample **1** suggests that the rod/flake like structures are composed of TiS_2 (At% 36% Ti, 64% S). and had average dimensions of 100-300 nm in width and around 2.5 μm in length. These structures closely resemble those seen from MOCVD growth of TiS_2 from a $TiCl_4$ precursor and a t-butyl sulfide sulfur source (at 500 ºC) [21]. Sample **2** however, showed no evidence of reaction or growth with only a low density of micro-particles of sulfur scattered on the Ti surface. In SAPVT the sulfur is transported as a reactive vapour and the reaction to form the chalcogenides occurs post-transport on the surface of the substrate likely *via* a vapour–solid (VS) or vapour-liquid-solid (VLS) mechanism. Given the small quantities of metal on the substrate - *ca*. 3×10^{-4} g; (6.26×10^{-6} moles Ti; a molar ratio of roughly 1 to 50 Ti : S) - even very small and/or localised changes in the conditions of the substrate surface, such as defects or impurities, would appear to have a profound influence on the nucleation and growth behaviour. Given the unpredictable outcome of these and other SAPVT reactions in the Ti-S system we considered options to improve reproducibility. Subsequent reactions combined titanium and sulfur as reactant powders to participate in anticipated SACVT reactions. In all but one of the cases summarised in Table 1, titanium powder was added at a l:2 Ti:S molar ratio and syntheses were performed as a function of temperature. Results from samples **3-9** were both reproducible and led to products that could be characterised, The first of these SACVT reactions was slow cooled and yielded **3**, which was revealed by SEM to consist of irregular fused submicron sized particles (Fig 3a). EDX gave Ti:S ratios of Ti 35% : S 65% for this sample and PXD produced a pattern that provided a convincing match to TiS_2 (Fig 3b). Reflections were indexed to TiS_2,

(hexagonal space group P-3*m*) with *a* = 3.411(2) Å *c* = 5.707(4) Å. **3** exhibited temperature independent diamagnetism between 2-300 K.

Figure 2 SEM image of **1** showing the rod/flake like particles of sample **1** (by contrast, sample **2** produced no discernable products despite identical reaction conditions.)

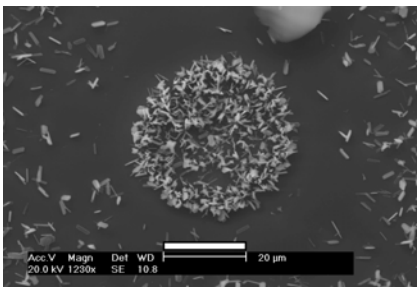

Figure 3 (a) SEM image of sample **3** and (b) its corresponding PXD pattern. Labelled reflections are those matching to TiS_2. The peak marked with an asterisk (*) originates from the underlying silica substrate.

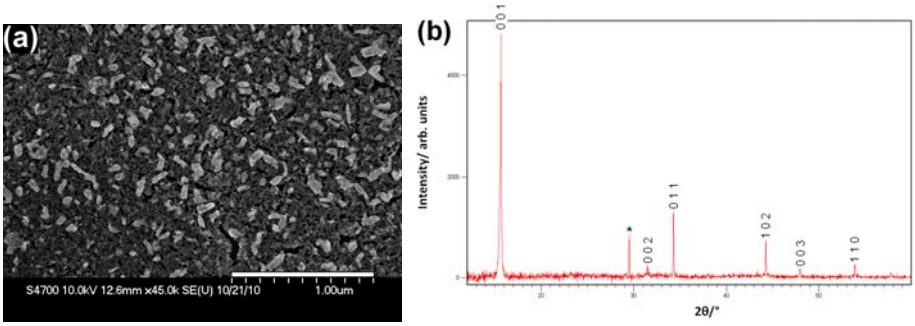

A systematic investigation of both temperature and time in which samples were quench-cooled from reaction temperature demonstrated that at 300 ºC (**4**) only S was found deposited at the surface of the substrate (Fig 4a and as evidenced from EDX spot scan data) whereas for higher temperatures (**5** - **8**) characterisation revealed that the morphology of the products changed dramatically for approximately constant composition (Fig 4b-e). At 400-500 ºC (**5** and **6)** flower like structures were formed which were tentatively characterised as TiS_2 according to elemental analysis from EDX (Ti 35% S 65%). Unfortunately PXD patterns of sufficient quality for **5** and **6** could not be obtained since the density of product on the substrate was such that any diffraction peaks were below background and dwarfed by scattering from the substrate. The flowers consisted of veil-like sheets some of which appeared to be electron transparent in high magnification SEM micrographs. (Fig 5). The magnetic susceptibility of **6** was weakly paramagnetic and temperature independent from 10 – 300 K with only a hint of a Curie tail below 10 K.

Figure 4, SEM Micrographs of products from reactions at a time of 24hrs, quenched in air. (a) 300 ºC (**4**) (b) 400 ºC (**5**) (c) 500 ºC (**6**) (d) 600 ºC (**7**) (e) 700 ºC (**8**)

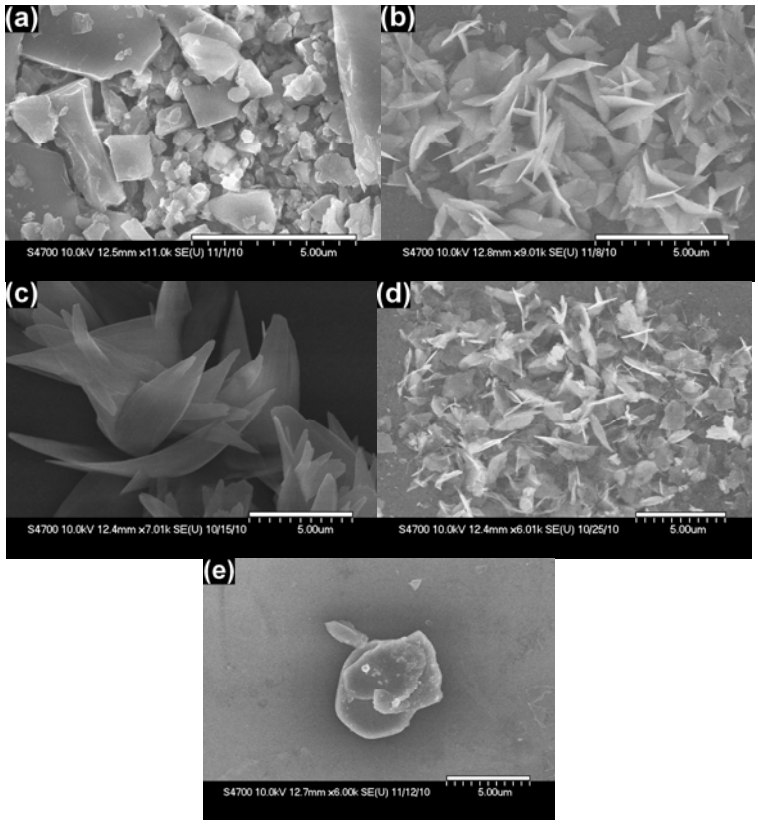

Figure 5, Higher magnification SEM micrographs of sample **6**, displaying (a) the electron transparent sheets that comprise the individual petals and (b) the thickness at the edges of these sheets,

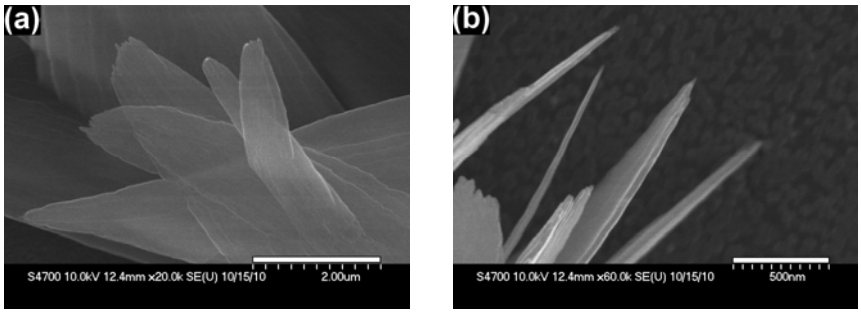

With a further increase in temperature (**7**-**8**), PXD indicates that TiS_2 is the principal phase (Fig 6). PXD patterns index to TiS_2, (hexagonal space group P-3*m*) with a = 3.405(7) Å c = 5.699(4) Å for **7** and a = 3.414(7) Å c = 5.702(8) Å for **8**. **7** in good

agreement with parameters reported for bulk stoichiometric materials (a =3.407 Å and c = 5.695 Å). [25]. Furthermore, with an increase in temperature the flower-like structures become less uniform and well-defined until at 700 °C (**8**) they are lost completely in favour of larger scale platelet crystallites, each of the order of 5-10 μm across (Fig 4e).

Figure 6 PXD comparison between samples **7** and **8**, showing that despite the evolution in morphology, the sulfide phase (and sample composition) remains the same.. Labelled reflections represent those matching TiS_2. Peaks marked with an asterisk originate from the underlying SiO_2 substrate.

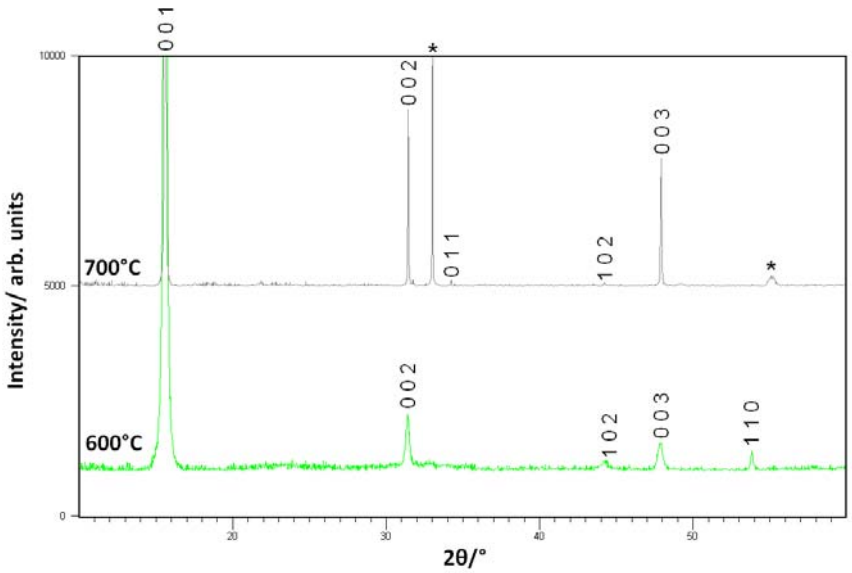

The Raman spectrum of **8** (Fig. 7) exhibits bands at 230 cm^{-1} and 330 cm^{-1} characteristic of TiS_2. Both bands are fairly broad but the latter is relatively intense. The two bands correspond to the E_g and A_{1g} phonon modes respectively and lie very close to the values seen in the bulk material (232 and 336 cm^{-1}) [26]. A further band is observed as a shoulder at 378 cm^{-1}. This broad peak has been observed previously in TiS_2 samples and while attributed to outcomes of Brillouin zone folding in superlattice of intercalated compounds such as Ag_xTiS_2, the feature is proposed to originate from second order, overtone effects in the unintercalated disulfide [27]. The broad peak at 378 cm^{-1} in **8**, however is surprisingly well resolved and there is even a hint of a second maximum close to *ca*. 420 cm^{-1}; these values are close to those for the G_1 and G_2 first order phonon modes in $Ag_{0.33}TiS_2$. Further SAED studies should help us determine if there is any evidence for superlattice formation in **8** and if so what is at the origin of such an ordering effect. Magnetic susceptibility measurements performed on **7** yield weakly paramagnetic behaviour that is essentially independent of temperature and displays no sign of magnetic ordering transitions. Unintercalated TiS_2 is expected to behave as a diamagnet (with core diamagnetic contributions outweighing Pauli paramagnetic effects) [28]. The positive susceptibility we observe could be a consequence of low level impurities, but given also the appearance of the Raman spectra, these data might suggest changes in the electronic structure of **7** and **8** relative to bulk stoichiometric TiS_2 (a 0.2 eV gap semiconductor

which becomes metallic for $Ti_{1.05}S_2$). Further studies of these materials are essential to understand the apparent variations.

Figure 7 Room temperature Raman spectrum of **8**, with a wavelength of exciting light of 532 nm.

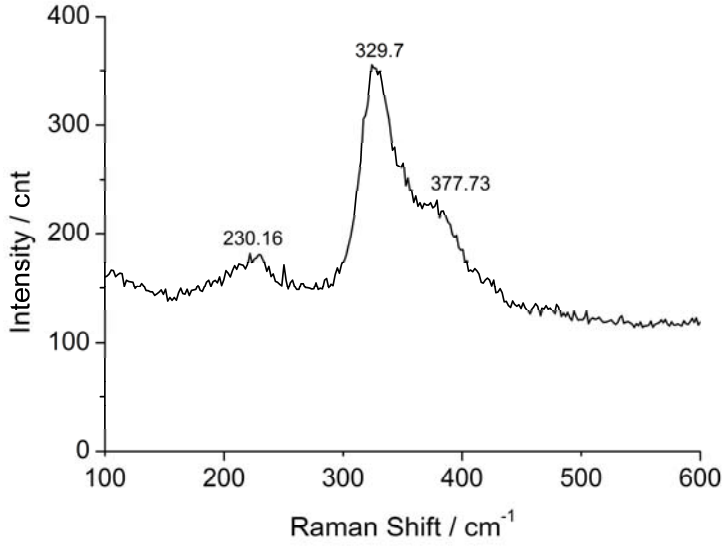

Finally we observed that if the Ti:S ratio is increased from 1:2 to 1:4 (**9**) while maintaining the reaction temperature at 500 ºC - the value where we previously observed "flower-like" growth for **6** - then one obtains results that contrast completely with 1:2 reactions (Fig 8). Although an approximately flower-like morphology is retained (in that "petal-like" structures appear to nucleate and grow from a central core), by contrast to **6**, sample **9** is composed of arrangements of radially distributed clusters of nanoribbons as opposed to the "petals" formed from nanosheets. The width of these ribbons can vary from tens of nm to several μm across. Irrespective of their width, these nanoribbons maintain electron transparency with thicknesses ranging from *ca*. 10-30 nm.

Figure 8, SEM micrographs of **9** (1:4 Ti:S ratio at 500 ºC and quenched) illustrating (a) cluster like growth from a central nucleation point; (b) the electron transparency of the ribbons the contrast between nanometer scale thicknesses and micron scale widths.

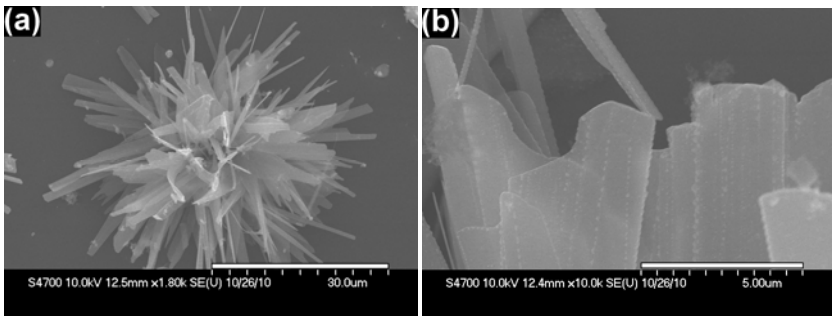

PXD of **9** revealed these structures to match more closely to TiS_3 than TiS_2 (Fig 9). The patterns observed for **9** bear a close resemblance to those from TiS_3 nanobelts [13] prepared at similar temperatures and indeed patterns of **9** can be tentatively indexed to the monoclinic $P2_1/m$ cell of TiS_3. EDX data would broadly support results from PXD although it should be noted that slighter lower S:Ti ratios than those expected from the trichalcogenide were consistently obtained; Ti:S 30 at% :70 at% (c.f 25 at% :75 at% for stoichiometric TiS_3). The morphology of the petals in clustered nanostuctures in **9** is more akin to the 1D nanostructures previously reported for transition metal trichalcogenides (MQ_3) [13], but whether the EDX data reflect a genuine departure from a stoichiometry of TiS_3 ($TiS_{3-\delta}$ or $Ti_{1+x}S_3$) remains to be determined. TiS_3 and related MQ_3 chalcogenides crystallise in monoclinic space group $P2_1/m$, forming structures in which chains of MQ_6 polyhedra propagate along the *b*-axis often resulting in profound anisotropic crystal growth. Such growth is often manifested in the microstructures of the trichalcogenides as elongated ribbons and needles of MQ_3 [11,29].

Figure 9, PXD pattern of sample **9**. Labelled reflections are those from monoclinic TiS_3, whereas open circles are peaks from the underlying silica.

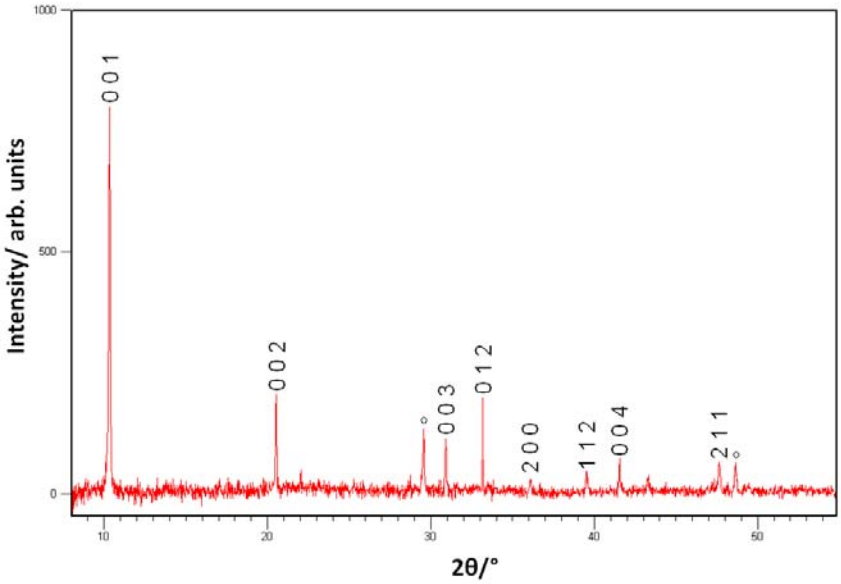

TEM studies showed that the TiS_3 ribbons shown in Figure 7 are micron size single crystals of nm scale thickness (Figure 10a), which yield well-defined diffraction patterns that can be matched to the monoclinic TiS_3 structure [12] (Figure 10b): the long axis of the ribbon is parallel to [010], and the thinnest direction is parallel to [001]. This reveals that the lowest energy surface of the crystal is the (001) face as would be expected from the crystal structure (since the structure contains chains of TiS_6 trigonal prisms connected by weaker Ti-S interactions to form sheets parallel to the (001) planes) and that the fastest growth on the most unstable surface must be happening along [010] directions corresponding to the propagation direction of the TiS chains in the TiS_3 structure. These observations are consistent with the growth of TiS_3 nanobelts reported previously [14].

Figure 10, Bright field TEM micrograph of a TiS_3 ribbon together with a selected area diffraction pattern from the same particle.

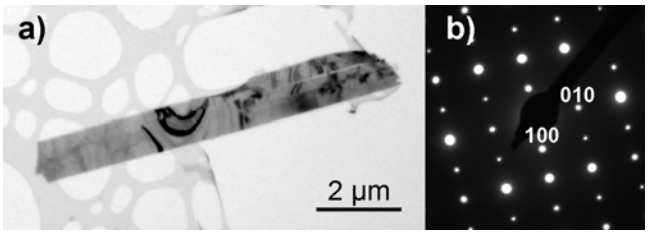

First reported in 1937 by Blitz, Ehrlich and Meisel [30] and with a crystal structure later determined in 1975 [12], titanium trisulfide forms tends to form below 560 °C. Titanium disulfide, TiS_2, is favoured above this temperature, usually as a result of trisulfide decomposition [31]. Investigations of powders and single crystals have established that TiS_3 is a weakly magnetic (and probably intrinsically diamagnetic) semiconductor (which can become extrinsically n-type [32-34]. The Raman spectrum of **9** (Fig. 11) exhibits four bands at 171 cm^{-1}, 296 cm^{-1}, 363 cm^{-1} and 553 cm^{-1} respectively which match well to the characteristic bands seen for bulk TiS_3 with each of the peaks corresponding to A_g k = 0 phonon modes.

Figure 11 Room temperature Raman spectrum of **9**, with a wavelength of exciting light of 532 nm.

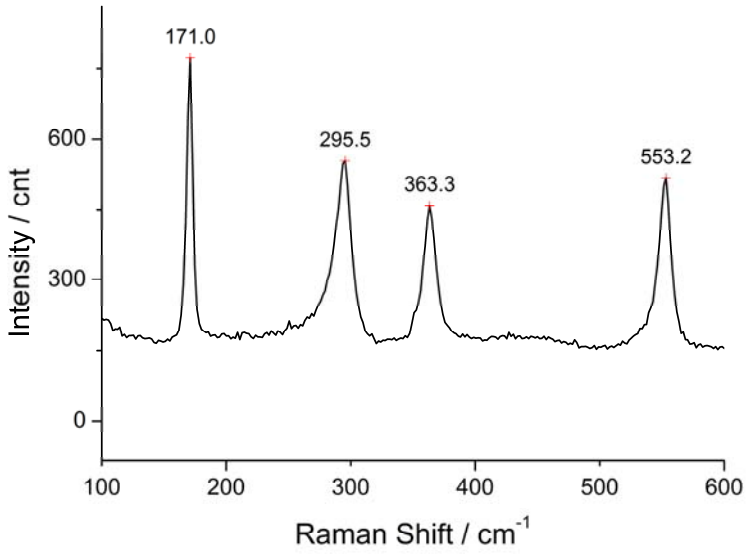

From the collection of results above, at low temperatures (300 °C; **4**) there is no perceptible reaction between the starting materials and the conditions lead only to transport and deposition of sulfur. For intermediate temperatures (400 - 500 °C), EDX

data consistently suggest that for higher Ti:S ratio samples we obtain products that match best to TiS_2. At temperatures above 500 ºC the EDX, PXD and Raman data indicate that the product of the 1:2 reactions is exclusively hexagonal CdI_2-type TiS_2 and as the reaction temperature is raised, so, unsurprisingly, the size of the crystalline TiS_2 platelets increase. Additionally, when employing a reaction temperature of 500 °C but decreasing the ratio of Ti:S to 1:4, the product becomes trisulfide, TiS_3, with a notable variation in morphology over the 1:2 product grown at the same temperature. At ambient pressure conditions one would expect from the Ti-S phase diagram that TiS_3 would decompose to TiS_2 + S at the peritectic at 632 ºC [35]. In actuality, the formation and stability of TiS_3 has been rationalised in the past in terms of empirical relationship linking sulfur partial pressure with (reaction) temperature (equation 1) [36].

$$\log P(\text{mm Hg}) = 10.42\ (\pm 0.42) - 6850/T\ (\pm 340) \quad (1)$$

Under similar experimental parameters to those used in this study (in terms of pressure and configuration), previous work indicated that the partial pressure of sulfur (assuming a 1:2 ratio) was not sufficient to prevent decomposition of TiS_3 to TiS_2 at 400 ºC [21]. These previous observations would agree with our own, albeit limited, data in that the elemental analysis (by EDX) of the nanostructures grown at both 400 ºC and 500 ºC would imply synthesis of sulfides closer to TiS_2 in stoichiometry than TiS_3. On decreasing the Ti:S ratio to 1:4, and hence increasing the S present in the system, the partial pressure at 500 ºC would appear to be sufficient to prevent decomposition. It is important to note however, that evidence from successful PVT reactions (**1**) shows that even with very high ratios of S to Ti (estimated at 50:1), elevated temperatures (650 ºC) lead to TiS_2 formation (and TiS_3 decomposition).

Previous studies of the formation of TiS_3 nanobelts from Ti foil and sulfur vapour had proposed that the trisulfide nanostructures grow *via* a vapour-solid mechanism in which gaseous TiS_x (formed between sulfur vapour and solid Ti at the interface) are the crucial species in nucleation and subsequent growth [13]. Our CVT studies would support this premise and in the case of **9**, TiS_x in the vapour phase is transported prior to deposition and further reaction (leading to growth at the substrate). It is not obvious from our studies, however, that TiS_3 is formed *in situ* in the course of the growth of TiS_2 in 1:2 reactions (**1**-**8**) which would require reduction and evolution of S (decomposition). From the very contrasting morphologies of the disulfide and trisulfide in these SACVT reactions, it is clear that such a transformation could not be pseudomorphic. Given previous precedent for pseudomorphic reduction of trisulfide precursors to disulfides (nanowires and nanotubes) [37], employing higher temperatures in 1:3 and 1:4 Ti:S reactions might be expected to produce similar pseudomorphic results in the Ti-S system, This offers the prospect of exerting control over trisulfide and disulfide dimensions and dimensionality (1D vs. 2D) by tailoring reaction temperature and reactant ratios (partial pressure). The ability to exert such control paves the way, potentially, to means of tailoring surface area and reactivity (for example, in gas and charge – lithium - storage applications) and size-mediated electronic structure and behaviour (and, for example, engineering optical band gaps).

Acknowledgements

This work was supported by EPSRC and WestCHEM. The authors would also like to thank Dr R. W. Hughes for assistance with PXD and Raman measurements and Miss H.J. Kitchen and Mr S. M. Hunter for assistance with the collection of SQUID data.

References

1 R. R. Chianelli., J. C. Scanlon., M. S. Whittingham., F. R. Gamble. (1975) 'Structural Studies of Intercalation Complexes $TiS_2.NH_3$ and $TaS_2.NH_3$', *Inorganic Chemistry.*, Vol. 14, No. 7, pp.1691-1696.

2 J. Dahn., R. R. Haering., (1979) 'Lithium Intercalation In TiS2', *Materials Research Bulletin.*, Vol. 14, No. 10, pp.1259-1262.

3 G. Scholz., P. Joensen., J. M. Reyes., R. F. Frindt. (1981) 'Intercalation Of Ag In TaS2 And TiS2', *Physica B & C.*, Vol. 105, No. 1-3, pp.214-217.

4 M. Inoue., H. Negishi., (1984) 'Chemical Vapor Growth And Manganese Metal Intercalation Of TiS2', *Journal of the Physical Society of Japan*., Vol. 53, No. 3, pp.943-946.

5 E. W. Ong., M. J. McKelvy., G. Ouvrard., W. S. Glaunsinger. (1992) 'Mercury Intercalates Of Titanium Disulfide - Novel Intercalation Compounds', *Chemistry of Materials*., Vol. 4, No. 1, pp.14-17.

6 M. Remskar., A. Popovic., H. I. Starnberg., (1999) 'Stacking transformation and defect creation in Cs intercalated TiS2 single crystals', *Surface Science*., Vol. 430, No. 1-3, pp.199-205.

7 H. E. Brauer., H. I. Starnberg., L. J. Holleboom., H. P. Hughes., V. N. Strocov. 'Modifying the electronic structure of TiS2 by alkali metal intercalation', (1999) *Journal of Physics-Condensed Matter*., Vol.11, No. 45, pp.8957-8973

8 Y. Tison., H. Martinez., I. Baraille., M. Loudet., D. Gonbeau. (2003) 'The specific behavior of MxTiS2 (x=1/4, M = Fe, Ni) surfaces probed by scanning microscopy (STM and AFM)', *Chemical Physics*., Vol. 290, No. 2-3, pp.267-278.

9 Chen, J., Li, S. L., Tao, Z.L., Shen, Y. T. (2003) 'Titanium disulfide nanotubes as hydrogen-storage materials', *J. Am. Chem. Soc.*, Vol. 125, No. 18, pp.5284-5285.

10 Chen, J., Tho, Z. L., Li, S. L. (2003) 'Lithium intercalation in open-ended TiS2 nanotubes', *Angew. Chem.-Int. Edit*, Vol. 42, No. 19, pp.2147-2151.

11 L. Brattas., A. Kjekshus. (1972) 'Properties of Compounds with Zrse3 Type Structure', *Acta Chemica Scandinavica*., Vol. 26, No. 9, pp.3441-3449.

12 S. Furuseth., L. Brattås., A. Kjekshus. (1975) 'Crystal-Structures of Tis_3, Zrs_3, $Zrse_3$, $Zrte_3$, Hfs_3, and $Hfse_3$', *Acta Chemica Scandinavica Series a-Physical and Inorganic Chemistry,* Vol. 29, No. 6, pp.623-631.

13 X. C. Wu., Y. R. Tao., Q. X. Gao. (2009) 'Preparation and Field Emission Properties of Titanium Polysulfide Nanobelt Films' *Nano Research.*, Vol. 2, No. 7, pp.558-564.

14 J. J. .Ma., X. Y. Liu., X. J. Cao., S. H. Feng., M. E. Fleet. (2006) 'Bundle of nanobelts up to 4 cm in length: One-step synthesis and preparation of titanium trisulfide (TiS3) nanomaterials', *European Journal of Inorganic Chemistry*, Vol. 3, pp.519-522.

15 Chen, J., Li, S. L., Tao, Z. L., Gao, F. (2003) 'Low-temperature synthesis of titanium disulfide nanotubes', *Chem. Commun.*, No. 8, pp.980–981.

16 Ma, J. J., Jin, H., Liu, X. Y., Fleet, M. E., Li, J. X., Cao, X. J., Feng, S. H. (2008) 'Selective Synthesis and Formation Mechanism of TiS2 Dendritic Crystals', *Cryst. Growth Des.,*Vol. 12, No. 8, pp.4460-4464.

17 Tao, Y. R., Wu, X. C., Zhang, Y. L., Dong, L., Zhu, J. J., Hu, Z. (2008) 'Surface-assisted synthesis of microscale hexagonal plates and flower-like patterns of single-crystalline titanium disulfide and their field-emission properties', *Cryst. Growth Des.*, Vol. 8, No. 8, pp. 2990-2994.

18 Prabakar, S., Bumby, C. W., Tilley, R. D. (2009) 'Liquid-Phase Synthesis of Flower-like and Flake-like Titanium Disulfide Nanostructures', *Chem. Mater.*., Vol. 21, No. 8, pp.1725-1730.

19 Zhang, Y., Li, Z. K., Jia, H. B., Luo, X. H., Xu, J., Zhang, X. H., Yu, D. P. (2006) 'TiS2 whisker growth by a simple vapor-deposition method', *J. Cryst. Growth*., Vol. 293, No. 1, pp.124-127.

20 C. W. Dunnill., H. K. Edwards., P. D. Brown., D. H. Gregory. (2006) 'Single-step synthesis and surface-assisted growth of superconducting TaS_2 nanowires', *Angew. Chem. Int. Ed.*, Vol. 45, No. 42, pp.7060-7063; C. W. Dunnill., I. MacLaren., D. H. Gregory., (2002) 'Superconducting tantalum disulfide nanotapes; growth, structure and stoichiometry', *Nanoscale*., Vol. 2, No. 1, pp.90-97.

21 Chang, H. S. W., Schleich, D. M, (1992) 'TiS_2 and TiS_3 Thin Films Prepared by MOCVD' *J. Solid State Chem.* Vol. 100, pp. 62-70.

22 H. K. Edwards., P. A. Salyer., M. J. Roe., G. S. Walker., P. D. Brown., D. H. Gregory. (2005) 'Metallic nanowires of Nb_3Te_4: A nanostructured chalcogenide', *Angew. Chem.-Int. Edit.*, Vol. 44, No. 23, pp.3555-3558. H. K. Edwards., P. A. Salyer., M. J. Roe., G. S. Walker., P. D. Brown., D. H. Gregory. (2005) 'Growth and microstructural characterization of single crystalline Nb_3Te_4 nanowires', *Cryst. Growth Des.*, Vol. 5, No. 4, pp.1633-1637.

23 S. J. Denholme., J. B. Gallagher., P. Dobson., J. M. R. Weaver., D. H. Gregory. (2010) 'New Surface-Directed, Vapour Transport Methods for the Controlled Growth of Nickel Sulfide Nanomaterials', Isr. J. Chem., Vol. 50, pp.515-523.

24 A. Boultif., D. Louer. (2004) *J. Appl. Cryst.* Vol. 37, pp.724-731. D. Louer., M. Louer. (1972) *J. Appl. Cryst.* Vol. 5, pp.271-275. A. Boultif., D. Louer. (1991) *J. Appl. Cryst*. Vol. 24, pp.987-993.

25 R. R. Chianelli,. J. C. Scanlon,. A. H. Thompson. (1975) 'Structure Refinement of Stoichiometric TiS_2', *Materials Research Bulletin.*, Vol. 10, No. 12, pp.1379-1382.

26 W. X. Unger, J. M. Reyes, O. Singh, A. E. Curzon, J. C. Irwin and R. F. Frindt. (1978) 'Raman Scauering in Ag-Intercalated TiS_2', *Solid State Commun*, Vol. 28 No. 1, pp. 109-112.

27 S. J. Sandoval. X. K. Chen, J. C. Irwin. (1992) 'Raman-Spectra of Ag_xTiS_2 and Lattice-Dynamics of TiS_2', *Phys. Rev. B*, Vol. 45., No. 24, pp. 14347-14353.

28 J. I. Meakin, P. C. Klipstein, R. H. Friend, (1987) 'Transport and Magnetic Properties of $Ag_{1/3}TiS_2$', *J. Phys. C*, Vol. 20, No. 2, pp. 271-276.

29 H. Hahn., B. Harder. (1956) 'Zur Kristallstruktur Der Titansulfide', *Zeitschrift Fur Anorganische Und Allgemeine Chemie.*, Vol. 288, No. 5-6, pp.241-256

30 W. Blitz., P. Ehrlich., K. Meisel. (1937) 'Über die Sulfide des Titans', *Z. anorg. Chem.,* Vol. 234, No. 2, pp.97-116.

31 F. K. Mctaggart., A. D. Wadsley. (1958) 'The Sulphides, Selenides, and Tellurides of Titanium, Zirconium, Hafnium, and Thorium .1. Preparation and Characterization', *Australian Journal of Chemistry.*, Vol. 11, No. 4, pp.445-457.

32 F. K. Mctaggart. (1958) 'The Sulphides, Selenides, and Tellurides of Titanium, Zirconium, Hafnium, and Thorium .3. Electrical Properties', *Australian Journal of Chemistry.,* Vol. 11, No. 4, pp.471-480.

33 H. Haraldsen., E. Rost., A. Kjekshus., A. Steffens. (1963) 'On Properties of TiS_3, ZrS_3, and HfS_3', Acta *Chemica Scandinavica.*, Vol. 17, No. 5, pp.1283-1292.

34 E. Finkman., B. Fisher. (1984) 'Electrical Transport Measurements in TiS_3', *Solid State Communications.,* Vol. 50, No. 1, pp.25-28.

35 J. L. Murray, (1986) 'The S-Ti (Sulfur-Titanium) System', *Bull. Alloy Phase Diagr.*, Vol. 7, No.2, pp. 156-163.

36 F. Tronc, M. Huber, (1969) 'Thermodynamic Properties of Titanium Trisulfide' *C.R. hebd. Seanc., Acad. Sci. Paris Ser. C.* Vol. 268, No. 20, p. 1771.

37. R Tenne, C. N. R. Rao, (2004) 'Inorganic nanotubes', *Phil. Trans. R. Soc. Lond.,* Vol. 362, pp. 2099-2125.